ORGANOMETALLICS

pubs.acs.org/Organometallics Article

Synthesis and Characterization of Co^{III}(TIM) Complexes Bearing Alkenyl or 1-Aza-2-cobalt-cyclopropane Moieties

Leobardo Rodriguez Segura, Kyle J. McGuire, Adharsh Raghavan, Jeremy J. Roos, and Tong Ren*

Cite This: *Organometallics* 2024, 43, 1057−1067 Read Online

ACCESS | Metrics & More | Article Recommendations | Supporting Information

ABSTRACT: Reported herein are the synthesis and characterization of mono- and bis-alkenyl Co^{III}(TIM) (TIM = 2,3,9,10-tetramethyl-1,4,8,11-tetraazacyclotetradeca-1,3,8,10-tetraene) complexes along with products containing a 1-aza-2-cobalt-cyclopropane unit. The *trans*-$[Co(TIM)(C(CH_2)Ar)Cl]^+$-type (Ar = phenyl (Ph, **1a**), $-C_6H_4$-4-^{t}Bu (**1b**), and $-C_6F_5$ (**1c**)), *trans*-$[Co(TIM)(C(CH_2)Ar)_2]^+$-type (Ar = Ph (**2a**) and $-C_6F_5$ (**2c**)), and *trans*-$[Co(TIM'')(C(CH_3)Ar)Cl]^+$-type complexes (Ar = Ph (**3a**) and $-C_6H_4$-4-^{t}Bu (**3b**); TIM″ is the resultant derivative of TIM) were prepared from the reaction between *trans*-$[Co(TIM)Cl_2]PF_6$ and the corresponding terminal aryl alkyne in the presence of $NaBH_4$. Molecular structures of **1a**/**c**, **2a**/**c**, and **3a** were established via single-crystal X-ray diffraction studies. Characterization using ^{1}H NMR further confirmed the occurrence of either an alkenyl (**1** and **2**) or 1-aza-2-cobalt-cyclopropane (**3**). The absorption spectra of **1** and **3** reveal differences in the optical HOMO−LUMO gaps with well-defined d−d bands at 477 and 512 nm for **1a** and **3a**, respectively. Cyclic voltammograms of **1** and **2** consist of an irreversible oxidation and an irreversible reduction characteristic of the Co^{III} center, while those of **3** display two reduction events. Density functional theory calculations were performed to investigate the bonding and electronic structures of **1a**−**3a**. Natural bonding orbital calculations on **3a** suggest significant stabilization in donor → acceptor resonance-type interactions afforded by the 1-aza-2-cobalt-cyclopropane unit.

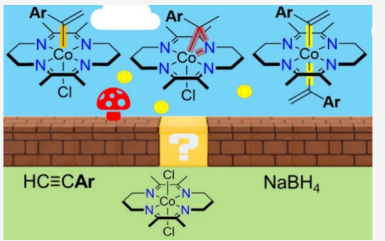

INTRODUCTION

The desire for a more sustainable chemical technology and cost concerns surrounding noble metals have led to increased efforts in developing catalysts based on earth-abundant elements, especially 3d metals, across academic and industrial settings.[1,2] Achieving this goal is complicated by the tendency of 3d metals to favor one-electron redox chemistry over the canonical two-electron redox processes mediated by the noble metals.[3] In this regard, redox noninnocent ligands offer a means to overcome such a complication by enabling two-electron redox events in 3d metal complexes.[4] Various Fe- and Co- pincer complexes have been demonstrated to catalyze a variety of organic transformations, such as alkene hydrogenation[5,6] and the asymmetric hydrofunctionalization of alkenes and alkynes,[7] as a testament to the success of employing redox active ligands.

Macrocyclic ligands consisting of multiple imine bonds represent another class of promising redox noninnocent scaffolds, and several examples of 3d metal complexes supported by such macrocycles have exhibited remarkable properties and reactivities. For example, Co^{II}-porphyrins have been utilized to promote carbene transfer reactions.[8] Additionally, the Hess laboratory reported the electrochemical production of hydrogen promoted by $Co^{III}(Mabiq)^{2+}$,[9] while $Co^{III}(Mabiq)Cl_2$ was capable of mediating the C3- and *N*-alkylation of indoles and indazoles via photoinduced Co−Cl homolysis.[10] A collaborative study by the laboratory of Vura-Weis and us revealed that an Fe-CN complex supported by a tetra-imine macrocycle significantly enhanced dπ−π*(C═N) interactions, yielding a record-long metal-to-ligand charge transfer lifetime (1.25 ns) for Fe(II) complexes.[11,12] While these reports did not directly invoke the redox noninnocence of the macrocycle, studies on Fe(TIM) complexes (TIM = 2,3,9,10-tetramethyl-1,4,8,11-tetraazacyclotetradeca-1,3,8,10-tetraene) demonstrated the ability of the tetra-imine macrocycle to undergo multiple one-electron reductions and to behave as an electron storage unit; therefore, the potential for noninnocent behavior.[13,14]

Recently, our laboratory carried out a series of studies based on the reactions between *trans*-$[Co(TIM)Cl_2]^+$ and alkynes (HC_2R). Under weak base conditions, *trans*-$[Co(TIM)Cl_2]^+$ reacts with HC_2R in the presence of NEt_3 to afford *trans*-$[Co(TIM)(C_2R)Cl]^+$, which is subsequently converted to *trans*-$[Co(TIM)(C_2R)(C_2R')]^+$ under similar conditions via a *trans*-$[Co(TIM)(C_2R)(NCMe)]^{+2}$ intermediate (Path **A** in Scheme 1).[15,16] Surprisingly, the reactions with more electron rich terminal alkynes, HC_2R (R = 4-*N*,*N*-dimethylaniline and ferrocene) under weak or strong base conditions afford both

Received: March 21, 2024
Revised: April 1, 2024
Accepted: April 4, 2024
Published: April 16, 2024

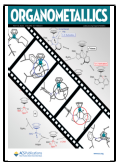

https://doi.org/10.1021/acs.organomet.4c00113
Organometallics 2024, 43, 1057−1067

Scheme 1. Previously Studied Reaction Pathways between *trans*-[Co(TIM)Cl_2]$^+$ and Terminal Alkynes[a]

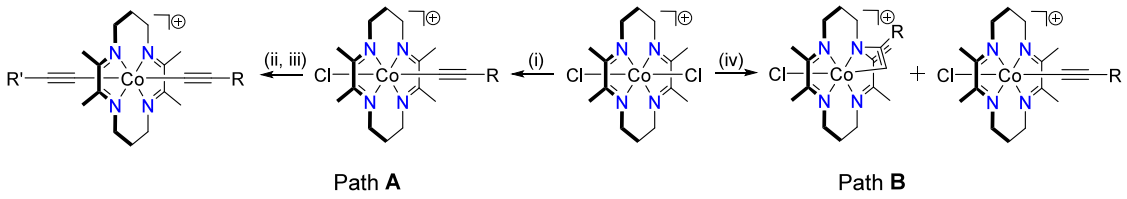

[a](i) HC_2R, Et_3N, MeOH. (ii) AgOTf, MeCN. (iii) HC_2R, Et_3N, MeCN. (iv) HC_2R, Et_3N or KOH, MeOH.

Scheme 2. Synthesis of 1−3; Ar = −Ph (a); $-C_6H_4$-4-^{t}Bu (b); $-C_6F_5$ (c)

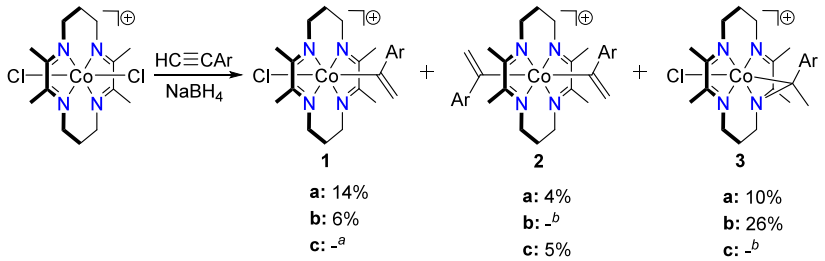

[a]Product was detected, but isolation was not successful. [b]Species was not detected in synthesis. [c]Isolated yields are reported from the one-pot reaction detailed in the Experimental Section.

Scheme 3. Plausible Pathways for the Formation of 1a−3a[a]

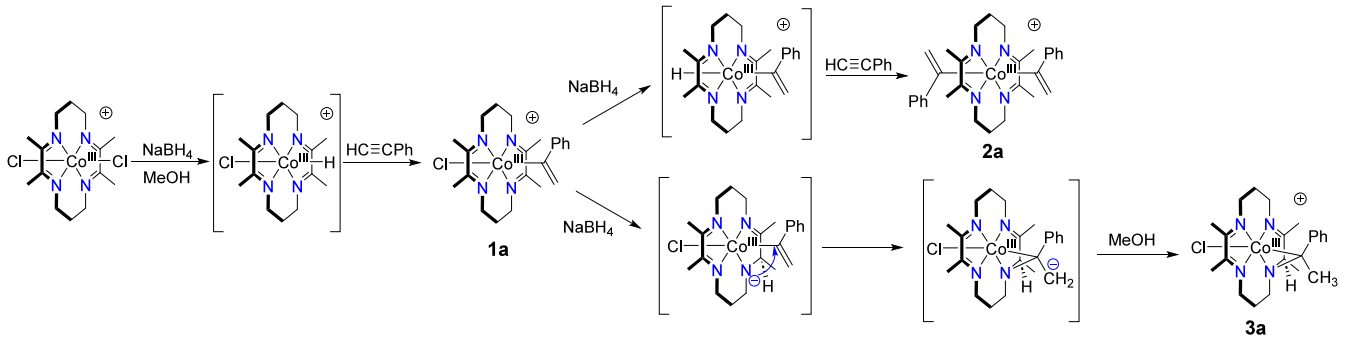

[a]Species in brackets are the speculated intermediates.

the expected *trans*-[Co(TIM)(C_2R)Cl]$^+$ and an unexpected *trans*-[Co(TIM′)((HC = C)R)Cl]$^+$ species bearing a 1-aza-2-cobalt-cyclobutene unit (Path **B** in Scheme 1).[17,18] The unique coordination of the alkynes in *trans*-[Co(TIM′)((HC = C)R)Cl]$^+$ was attributed to an unexpected reactivity involving the TIM ligand, which could be accessed upon the deprotonation of a TIM methyl group to trigger an intramolecular rearrangement generating the four-membered ring. Notably, the resulting products in these reactions were constitutional isomers of the anticipated α-alkynyl complexes, *trans*-[Co(TIM)(C_2R)Cl]$^+$.[15] Contemporary to our work, Fe azametallacyclobutene complexes were studied by the group of Neely, where the Fe species underwent interesting insertion reactions with nitrile and terminal alkyne.[19,20]

Inspired by recent efforts on the catalytic application of vitamin B_{12} and related model complexes in cobalt-mediated radical reactions[21] and hydrogen atom transfer reactions,[22] we sought to generate Co(TIM) organometallic compounds featuring Co−C_{sp2} bonds instead of Co−C_{sp} bonds. Thus, the reactions between *trans*-[Co(TIM)Cl_2]$^+$ and HC_2R in the presence of $NaBH_4$ result in new mono- (**1** in Scheme 2) and bis-alkenyl (**2**) Co^{III}(TIM) compounds. Intriguingly, a third product bearing a 1-aza-2-cobalt-cyclopropane (**3**) was also identified and isolated, and its formation revealed a new noninnocent behavior of the TIM ring that differs from the previously reported reactivities. Described in this contribution are the syntheses of these products and their structural, spectroscopic, and electrochemical characterizations.

RESULTS AND DISCUSSION

Synthesis. The reaction between *trans*-[Co(TIM)Cl_2]PF_6 and 2 equiv of $NaBH_4$ in the presence of excess phenylacetylene leads to the formation of three unique species: *trans*-[Co(TIM)(C(CH_2)Ph)Cl]PF_6 (**1a**), *trans*-[Co(TIM)(C(CH_2)Ph)$_2$]PF_6 (**2a**), and *trans*-[Co(TIM″)(C(CH_3)Ph)Cl]PF_6 (**3a**) (TIM″ is the resulting derivative of TIM). Separation of the products could be achieved through column chromatography using a gradient of CH_3OH/CH_2Cl_2; however, their gradual degradation on silica makes bulk purification via this method limiting. To overcome these purification difficulties, the selective formation of each product was attempted by altering the molar equivalents of the reagents used. It was found that the use of 1.5 mol equiv of $NaBH_4$ led to an improved selectivity for **1a**. Increasing the molar equivalence of $NaBH_4$ led to an increase in formation of **3a**, while a large excess of phenylacetylene (>10 mol equiv)

https://doi.org/10.1021/acs.organomet.4c00113
Organometallics 2024, 43, 1057−1067

favored the formation of the bis-alkenyl product, **2a**. Full details of these conditions can be found in the Supporting Information. In all three product types, the complexes are stable in the solid state and in solution; however, in the latter phase, care was taken to avoid extended exposure to ambient light as some degradation was observed after several hours unless kept in the dark.

Insights into the plausible pathways for the formation of product **1a** can be gleaned from previous studies detailing the reaction between structurally analogous organocobalt(III) systems like cobalamins[23] and Co-porphyrins[24] with phenylacetylene. As shown in Scheme 3, the reaction between $[Co(TIM)Cl_2]PF_6$ and $NaBH_4$ is postulated to generate a Co^{III}−H species. Subsequently, the transient $[H\text{-}Co^{III}(TIM)]^+$ intermediate undergoes a *cis*-addition of the hydrogen to the terminal alkyne at the α-carbon to yield the Markovnikov product, **1a**. Interestingly, in the case of cobaloximes, Schrauzer et al. also report the formation of a *trans*-addition product resulting from a nucleophilic attack at the β-carbon of the alkyne by a Co^I intermediate.[25] Ensuing studies suggested that the Co^I and Co^{III}−H species exist in a highly pH-sensitive equilibrium wherein alkaline conditions could be employed to shift the equilibrium toward the Co^I intermediate.[26] However, the lack of an observable *trans*-$[Co(TIM)(CHCHPh)Cl]^+$-type product, even under basic conditions, suggests that a $Co^I(TIM)$ intermediate is not present in the TIM-based system.

The formation of compound **2a** is expected to follow a pathway similar to that of **1a**. Excess $NaBH_4$ in solution further reacts with **1a** to generate a $[H\text{-}Co^{III}(TIM)(C(CH_2)Ph)]^+$ intermediate, which reacts with excess HC_2Ph to yield the bis-alkenyl product. Such a pathway is supported by the reported synthesis of *trans*-$[Co(TIM)(CH_3)_2]BPh_4$ by Farmery and Busch in which *trans*-$[Co(TIM)(CH_3)I]BPh_4$ was reduced via sodium amalgam to obtain an isolable neutral $Co^I(TIM)(CH_3)$ species as an intermediate.[27] Notably, with the exception of *trans*-$[R_2Co((DO)(DOH)pn)]^+$-type complexes (R = alkyl; (DO)(DOH)pn = 2,2′-(1,3-diaminopropanebis(2-methyl-3-butanone)oxime)),[28] other vitamin B_{12}-model organocobalt complexes bearing dialkyls have not been reported.

In product **3a**, the unusual coordination reveals a unique reactivity and an alternative reaction pathway than proposed for **2a**. Organocobalt complexes supported by imino/oxime ligands which bear a N−Co−C three-membered ring have been reported.[29−32] However, the aza-cobalt-cyclopropane moiety for these complexes is formed through the deprotonation of an imine methyl group to yield a deprotonated enamine intermediate, which undergoes ring closure upon reaction with an axially coordinated halogenated alkyl ligand.[32] Other aza-cobalt-cyclopropanes have been synthetically obtained via the photoinduced decarboxylation of amino acids coordinated to cobalt(III) centers.[33−36]

Instead, the reaction conditions employed (i.e., the use of $NaBH_4$) can lead to the reduction of an imine unit within the TIM ring, as shown in Scheme 3. The resulting nucleophilic nitrogen is capable of attacking at the axially coordinated alkenyl ligand to generate the titular three-membered ring. The transient carbanion intermediate readily deprotonates a methanol molecule to complete the formation of **3a**. The detection of a trace amount of a tri-imine/monoamine derivative of **1a** ($[Co(TIM'')(C(CH_2)Ph)Cl]PF_6$; **1a′**) using ^1H NMR (see the Nuclear Magnetic Resonance section below) suggests that the intermediate bearing the nucleophilic amine can also deprotonate a methanol molecule to inhibit the formation of **3a**. Also, it is plausible that a cobalt carbene intermediate is formed from the protonation of the Co-vinyl, and undergoes migratory insertion to form **3a**, analogous to the established literature precedents of metal carbene insertions.[37−39]

To test the electronic influence of the −Ar moiety, the reaction between $[Co(TIM)Cl_2]PF_6$ and 3 mol equiv of HC_2Ar (Ar = $-C_6H_4$-4-^{t}Bu or $-C_6F_5$) in the presence of 2 mol equiv of $NaBH_4$ was performed. Upon the introduction of a *para-tert*-butyl group, the mono-alkenyl product, *trans*-$[Co(TIM)(C(CH_2)C_6H_4\text{-}4\text{-}^tBu)Cl]PF_6$ (**1b**), and *trans*-$[Co(TIM'')(C(CH_3)C_6H_4\text{-}4\text{-}^tBu)Cl]PF_6$ (**3b**) were exclusively observed. The formation of a bis-alkenyl analogue of **2a** was not observed despite employing either 5 mol equiv of the terminal alkyne or longer reaction times. The slightly increased electron donating capabilities of the ^{t}Bu group favor the reduction of a TIM imine group, and subsequent formation of **3b**, over the formation of a $[H\text{-}Co^{III}(TIM)(C(CH_2)C_6H_4\text{-}4\text{-}^tBu)]^+$ intermediate. In the case of the electron-withdrawing terminal alkyne $HC_2C_6F_5$, the dominant products are *trans*-$[Co(TIM)(C(CH_2)C_6F_5)Cl]PF_6$ (**1c**) and *trans*-$[Co(TIM)(C(CH_2)C_6F_5)_2]PF_6$ (**2c**). The lack of an observed aza-cobalt-cyclopropane-bearing analogue reveals the favorability of a transient $[H\text{-}Co^{III}(TIM)(C(CH_2)C_6F_5)]^+$ intermediate over the reduction of the TIM ligand. Interestingly, *trans*-$[Co(TIM'')(C(CH_2)C_6F_5)Cl]PF_6$ (**1c′**, see Figure S1), in which an iminyl group is hydrogenated to yield the tri-imine/monoamine system, has been identified as a minor product and further supports the proposed reaction pathway for the formation of the metallacycle (**3**) discussed above. Seemingly, the electron-withdrawing nature of the aryl results in increased electron donation from the Co(III) center to the bonded carbon such that the latter is a weaker electrophile than when Ar = −Ph or $-C_6H_4$-4-^{t}Bu; thus, the formation of the tri-imine/monoimine species, **1c′**, is preferred over an analogue of **3**. Unfortunately, extensive efforts to cleanly isolate **1c** from **1c′** have proven unsuccessful due to nearly identical R_f values in a variety of solvent mobile phases.

An effort to study the reaction using $HC_2C_6H_4$-4-NO_2 as an alternative electron-deficient alkyne was unsuccessful, likely because the nitro group is a strong electrophile and capable of reacting with borohydride. Other reaction attempts with HC_2Fc (Fc = ferrocene) and $HC_2C_6H_4$-4-NMe_2 as electron-rich terminal alkynes did not yield any identifiable products. Attempts to use zinc as a reducing agent milder than $NaBH_4$ also proved to be ineffective. Unlike the success of using granulated Zn that has been observed with cobaloximes and cobalamins,[40] the reduction of $[Co(TIM)Cl_2]^+$ with Zn is sluggish and ultimately results only in the degradation of the starting material. The reactivity of $[Co(TIM)Cl_2]PF_6$ with internal alkynes, namely, 3-propyne and diphenylacetylene, was also tested. The reaction between 2 mol equiv of $NaBH_4$ and $[Co(TIM)Cl_2]^+$ generated the blue reaction mixture described above. However, there was no further color change to suggest reaction with alkyne. Analysis of the reaction mixture via ESI-MS did not identify any expected product from the reaction between $[Co(TIM)Cl_2]PF_6$ and the internal alkynes. Experimental details of the attempted reactions are provided in the Supporting Information.

Structural Characterization. The molecular structures of **1a**/**c**, **2a**/**c**, and **3a** (shown in Figures 1−3) were determined by using single-crystal X-ray diffraction, and selected bond

https://doi.org/10.1021/acs.organomet.4c00113
Organometallics 2024, 43, 1057−1067

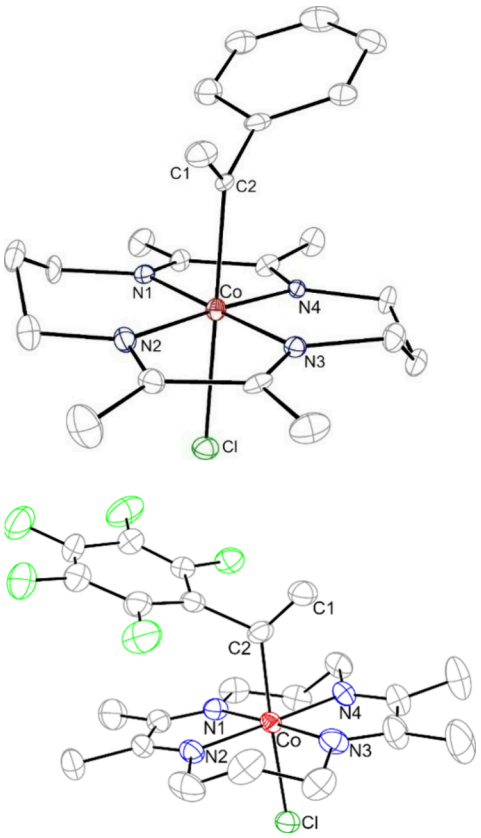

Figure 1. ORTEP plot of **1a** (top) and **1c** (bottom) at the 30% probability level. H atoms, solvates, disorder, and counteranions are omitted for clarity.

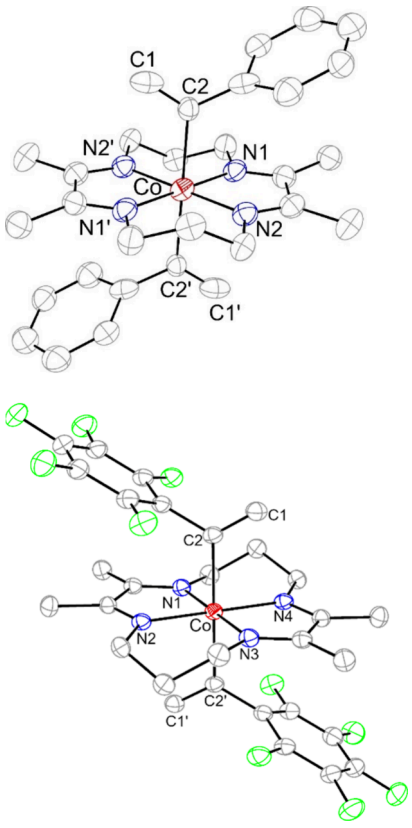

Figure 2. ORTEP plot of **2a** (top) and **2c** (bottom) at the 30% probability level. H atoms, solvates, disorder, and counteranions are omitted for the sake of clarity.

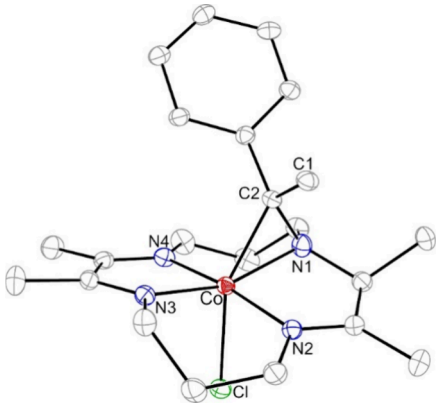

Figure 3. ORTEP plot of **3a** at the 30% probability level. H atoms, solvates, disorder, and the counterion are omitted for the sake of clarity.

lengths and angles are given in Table 1. Additional details regarding data collection and structure refinement can be found in the Supporting Information (Tables S1 and S2). In all structures, the Co(III) centers adopt a pseudo-octahedral geometry with the nitrogen atoms occupying the equatorial ligands and either chloro, alkenyl, or alkyl ligands occupying the axial positions. In the structures of **1a** and **1c** (Figure 1), the alkenes (C═C bond lengths of 1.305(3) and 1.272(8), respectively) are coordinated to the cobalt center at the α-carbon, in accordance with a *trans* addition of the H−Co^{III}(TIM) to the terminal alkyne, as described above.[25] The Co−C bond in **1a** has a bond length of 2.044(2) Å, which is elongated compared to the Co−C bond of analogous co^{III}balamin[23] (2.004(8) Å) and Co^{III}(TAP)[24] (TAP = 5,10,15,20-tetrakis(*p*-methoxyphenyl)porphyrin) (1.969(5) Å) complexes. Additionally, while the structure of an analogous α-styrenyl derivative of cobaloximes has not been reported, the related (4-^{t}Bu-py)$Co^{III}(DMG)_2$ bearing an axial α-bonded diene has a Co−C bond length of 1.954(15) Å.[41] The significant elongation in the Co−C bond length for **1a** is most likely a direct result of the *trans* axial chloro ligand, since the Co^{III}(porphyrin) complexes lack a *trans* coordinated ligand to the alkenyl and the cobaloximes and cobalamins bear neutral, π-accepting bases in the *trans* axial position. In complex **1c**, a contraction of the Co−C bond (1.999(6) Å) is also observed; however, this may be attributed to the electron-withdrawing nature of $-C_6F_5$. The electronic influences are further illustrated by the increased Co−Cl bond distances in **1a** (2.3541(8) Å) relative to **1c** (2.3073(9) Å), which is a result of the more electron-rich phenyl group exerting a greater *trans* influence across the Co center in **1a**.

Upon the coordination of a second alkenyl moiety in **2a** (Figure 2), the Co−C bond distance is elongated to 2.12[1] Å (averaged over two independent moieties) due to an increased *trans* influence. A similar elongation is observed for that of **2c** (2.074(2) Å) (Figure 2). Interestingly, both **2a** and **2c** possess a center of inversion at the Co^{III} site, which results from the aryl moiety being positioned toward one of the di-imine moieties of the TIM macrocycle. It is known for cobaloximes that alkyl ligands bearing bulkier substituents are less stable due to steric hindrance from the macrocycle;[42] therefore, it is

https://doi.org/10.1021/acs.organomet.4c00113
Organometallics 2024, 43, 1057−1067

Table 1. Selected Bond Lengths (Å) and Bond Angles (°) for $[1a]^+$, $[1c]^+$, $[2a]^+$, $[2c]^+$, and $[3a]^+$

	$[1a]^+$	$[1c]^+$	$[2a]^a$	$[2c]^+$	$[3a]^+$
Co−Cl	2.3541(8)	2.3073(9)			2.3648(8)
Co−C2	2.044(2)	1.999(6)	2.177[9]	2.075(4)	1.967(2)
C1−C2	1.305(3)	1.272(8)	1.253[10]	1.324(4)	1.518(3)
N1−C2					1.496(3)
Co−N1[b]	1.916[3]	1.916[6]	1.89[1]	1.905[3]	1.927(2)
N1−Co−C2[c]	90.9[1]	90.5[4]	89.8[6]	90.4(1]	45.19(9)
Co−C2−N1					66.0(1)
C2−N1−Co					68.8(1)
Cl−Co−C2	179.24(5)	176.9(2)			149.74(7)

[a]Averaged over two independent moieties. [b]For **1** and **2**, Co−N_{av} is reported. [c]N_{av}−Co−C2 is reported for **1** and **2**.

possible that the fluxional propylene bridges on the TIM macrocycle[43] lead to the locked positions of the aryl moieties observed in the solid state.

The coordination of the axial ligand in **3a** (Figure 3) is starkly different than those in **1a** and **2a**. The formation of the three-membered moiety results in a Co−C bond length of 1.967(2) Å and a new C−N bond with a bond length of 1.496(3) Å. The latter bond, coupled with the reduction of the imine unit to an amine at N1−C9 (1.460(3) Å), leads to a loss of planarity of the TIM ring with N1 laying above the equatorial plane and toward the axial ligand. The Co−C bond length is slightly elongated relative to other known aza-cobalt-cyclopropane bearing complexes.[29−33,36] Similarly, the C−N bond is elongated, while the Co−N (1.927(2) Å) bond is contracted. Noteworthy, the previously reported analogous structures typically possess a neutral-type ligand in the *trans* coordination site and an unsubstituted carbon atom within the macrocycle. Plausibly, a combination of the *trans* influence exerted by the chloride ligand and the steric hindrance of the phenyl ring in **3a** leads to the observed variations.

Nuclear Magnetic Resonance. ^{1}H NMR studies were employed to aid in the identification of the complexes based on diagnostic signals afforded by the varying coordination modes (for spectra, see Figures S2−S7). The NMR spectrum of **3a** in CD_3CN is indicative of a compound possessing low symmetry and has a highly identifiable $\delta(-CH_3)$ signal at 1.07 ppm, which is assigned to the methyl group of the reduced alkenyl moiety. In the *tert*-butyl functionalized complex, **3b**, the corresponding signal appears at 1.06 ppm, suggesting a negligible electronic influence of the *tert*-butyl group on the methyl. Moreover, the reduction of an imine unit in the TIM ligand leads to a considerable upfield shift in the protons of the adjacent methyl group, and the spectra of **3a** and **3b** display a well-resolved doublet signal at 1.73 ppm. Definitive assignment of this signal enables the identification of the tri-imine/monoamine byproducts, **1a′** and **1c′**, which bear an analogous signal at 1.57 and 1.59 ppm, respectively (see Figure S8).

For complex **1**, two alkenyl proton signals can be observed at 3.88 and 4.23 ppm. Likewise, these signals appear at 3.86 and 4.24 ppm for **1b**. The NMR spectra for **1a** and **1b** feature splitting of the propylene proton signals (3.60−3.90 ppm). This is expected for species bearing two different *trans* ligands, in which the $-CH_2CH_3CH_2-$ moieties can fluctuate above or below the plane of the TIM ligand. In contrast, in complex **2a**, which possesses higher symmetry, these protons are equally influenced by the alkenyl ligands. As a result, splitting of the propylene proton signals is not observed, and a well-defined triplet can be identified at 3.50 ppm. In **2c**, the corresponding signal is slightly shifted downfield to 3.56 ppm. The alkenyl protons in the latter experience a pronounced effect from the electron-withdrawing influence of the $-C_6F_5$ evident by the $\delta(CH_2)$ signals at 4.34 and 5.21 ppm while these appear at 3.81 and 4.97 ppm, respectively, for **2a**.

Electronic Absorption Spectra. Absorption spectra of **1a−3a** were collected in CH_3CN and are shown in Figure 4.

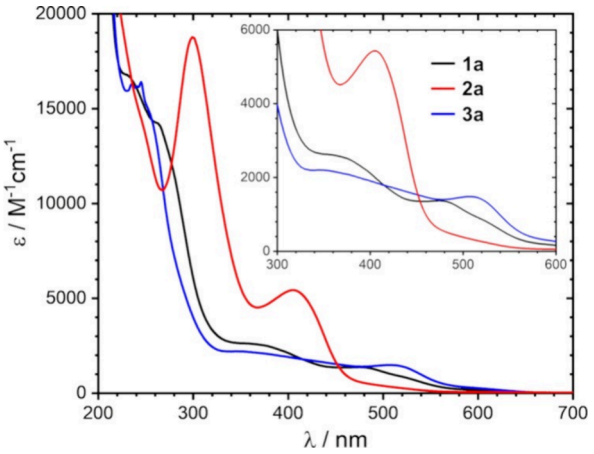

Figure 4. Absorption spectra of complexes **1a−3a** in CH_3CN. The d−d bands are shown in the inset.

Compound **2a** displays an intense ligand-based π(Ar) → π^*(Ar) transition at 300 nm. While analogous transitions are absent for **1a** and **3a** in the UV region, these compounds exhibit well-defined d−d transitions ($^1A_{1g} \rightarrow {}^1T_{1g}$, O_h) at 477 and 512 nm, respectively. In compound **2a,** the transition at 406 nm is tentatively assigned as a d−d band, which is substantially blue-shifted from that of **1a** due to a greatly enhanced ligand field with a second alkenyl ligand. The relatively high molar absorptivity (5400 M^{-1} cm^{-1}) suggests that this transition may have significant charge transfer character. The $-C_6F_5$ analogue, **2c**, displays a broad, ligand-based π(Ar) → π^*(Ar) transition at 272 nm (Figure S9) with no transition at lower energy levels. It is likely that the electron-withdrawing nature of the ligand in **2c** leads to a substantial blue-shift of the corresponding charge transfer band in **2a** causing it to become obscured by the more intense π(Ar) → π^*(Ar) transition. Due to the minimal influence of the *tert*-butyl group, the spectra of **1a** and **1b** are nearly identical, as are those of **3a** and **3b** (see Figure S10).

Electrochemical Studies. Voltammetric studies of the Co(III) complexes were conducted in CH_3CN, and their electrode potentials (vs $Fc^{+1/0}$) are listed in Table 2. Within the solvent window, an irreversible 1 e^- oxidation ($Co^{4+/3+}$) can be

https://doi.org/10.1021/acs.organomet.4c00113
Organometallics 2024, 43, 1057−1067

Table 2. Electrode Potentials of All Observed Redox Couples (V vs Fc^+/Fc) in 1a−3a[a]

	E_{pa} ($Co^{4+/3+}$)	$E_{1/2}$ ($Co^{3+/2+}$)	$E_{1/2}$ ($TIM^{0/-1}$)
1a	1.32	−1.01(0.17)[b]	
1b	1.35	−1.01(0.16)[b]	
2a	0.78	−1.83[c]	
2c	1.34	−1.61[c]	−2.11[c]
3a	1.14	−1.42(0.10)[b]	−1.56(0.06)
3b	1.12	−1.43(0.15)[b]	−1.57(0.07)

[a]Solutions contain 1.0 mM analyte and 0.1 M *n*-Bu_4NPF_6 as the supporting electrolyte in CH_3CN. Peak separation (ΔE_p) for reversible processes shown in parentheses. [b]Quasi-reversible couple. [c]Irreversible couple, E_{pc}, is reported.

observed for **1a** and **2a**, as shown in Figure 5. The oxidation in **2a** (0.78 V) is cathodically shifted relative to the same couple

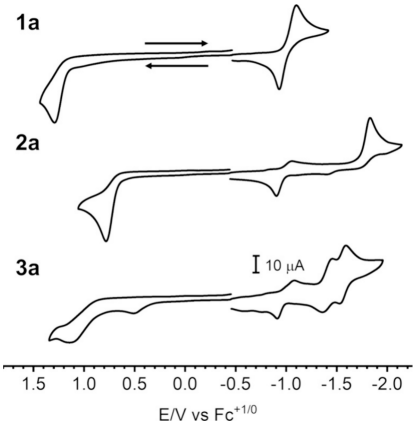

Figure 5. Cyclic voltammogram scans of 1.0 mM solutions of **1a** (top), **2a** (middle), and **3a** (bottom) in a 0.1 M solution of *n*-Bu_4NPF_6 in CH_3CN at scan rate = 0.1 V/s.

in **1a** (1.32 V) due to the replacement of the chloro ligand with a more electron donating alkenyl ligand. The use of a highly electron-withdrawing alkenyl ligand in **2c** significantly shifts the $Co^{4+/3+}$ oxidation to 1.34 V, in agreement with the stabilizing effects of the $-C_6F_5$ moieties discussed in the electron absorption studies above. In the case of **3a**, irreversible oxidation ($Co^{4+/3+}$) occurs at 1.14 V.

In the cathodic window, compounds **1a** and **3a** exhibit a quasi-reversible 1 e^- reduction ($Co^{3+/2+}$), while compound **2a** displays only an irreversible event. The reduction for **1a** occurs at −1.01 V, while the reduction of the bis-alkenyl compound **2a** is cathodically shifted to −1.83 V, in agreement with the trend observed in the $Co^{4+/3+}$ events. The application of more negative potentials results in several ill-defined reductions for both **1a** and **2a**. This is in contrast to previously studied Co(TIM) alkynyl complexes,[15] in which either two or one TIM ligand-based reductions were observed within the solvent window. This suggests that the Co(TIM) alkenyl complexes are less stable than their alkynyl counterparts. The redox potentials for the mono-alkenyl complexes also appear to be sensitive to the electronic properties of the Ar moieties. As discussed above, such an influence is minimal in the *tert*-butyl substituted complex, **1b** (Figure S11). However, as shown in Figure S12, the $-C_6F_5$ bis-alkenyl analogue, **2c**, exhibits a significantly shifted $Co^{3+/2+}$ potential at −1.61 V. Moreover, a TIM-based reduction can be observed for **2c** at −2.11 V.

In compound **3a**, the $Co^{3+/2+}$ reduction is displayed at −1.42 V. The near 0.40 V cathodic shift relative to **1a** can be attributed to the increased electron density around the cobalt center imbued by the aza-cobalt-cyclopropane. Interestingly, a second reversible event can be observed in the case of **3a** at −1.56 V, which can be tentatively assigned as a TIM″-based reduction. The corresponding reductions occur at −1.43 and −1.57 V for **3b**, as shown in Figure S11. Notably, the TIM-based reductions in previously reported aza-cobalt-cyclobutene-bearing Co(TIM) complexes occur at highly negative potentials (ca. −2.4 V),[18] indicating that the electronic influences imbued by the four-membered ring on the macrocycle are significantly different than those imparted on the macrocycle by the three-membered ring in **3a**.

Computational Studies. The bonding and electronic structures of **1a**, **2a**, and **3a** were investigated using density functional theory (DFT) calculations, and individual atomic contributions to the canonical MOs on the natural atomic orbital (NAO) basis were assessed through natural bonding orbital (NBO) calculations. The frontier MO diagrams (Figure S15) show that the five 3d orbitals mix significantly with both the axial and equatorial ligands in all three complexes. In view of the rarity of the three-membered cobalt aza-cyclopropane unit, a more localized description of the bonding situation in all three complexes (**1a**−**3a**) is provided. NBO calculations revealed that the Co−C bonding in **1a**−**3a** is clearly of σ-type (Tables S3−S5), and stronger σ-bonding axial ligands (alkenyl) in **2a** result in a greater *trans* influence than the chloro ligand in **1a**, as seen from the differences in the Mayer Bond Order (MBO) of the Co−C bond (0.81 in **1a** vs 0.62 in **2a**).[44]

Turning to the NBOs relevant to the metallacycle, the most significant donor → acceptor resonance-type interactions and their stabilization energies calculated from second order perturbation theory (SOPT; $E^{(2)}$) for **3a** are shown in Figure 6, wherein the metal hybrid orbitals are written as sd^{μ}, and C and N hybrids are written as sp^{λ} (λ, $\mu > 0$). At 106 kcal/mol, the largest resonance stabilization in **3a** lies within the metallacycle in the form of a geminal $\sigma_{Co-C2} \rightarrow \sigma^*_{Co-N1}$ interaction, while the corresponding interactions in **1a** and **2a** are roughly half this value, at 45 and 53 kcal/mol, respectively (Table S9). Similarly, the stabilization energy derived from $\sigma_{Co-N1} \rightarrow \sigma^*_{Co-C2}$ interaction in **3a** (53 kcal/mol) is more than twice the energy of the corresponding interactions in **1a** (21 kcal/mol) and **2a** (23 kcal/mol). Going from **1a** to **3a**, the pyramidalization of the axial carbon C2 and the formerly iminyl nitrogen N1 causes a drastic change in the hybridization of the orbitals involved in Co−C2 and Co−N1 NBOs; both C2 and N1 orbitals gain a significant amount of p-character. For the Co−C2 NBO, whereas in **1a**, Co and C2 employ $\sim sd^{2.6}$ and carbon $\sim sp^{3.1}$ hybrids, in **3a** they respectively employ $\sim sd^2$ and $sp^{5.9}$ hybrids (Table S9 and Figure 6). Similarly, in **1a**, Co and N1 orbitals are $sd^{1.8}$ and $sp^{2.5}$ hybridized whereas in **3a**, they are respectively $\sim sd^2$ and $sp^{7.8}$ hybrids. The large deviation from the nominal "sp^3" hybridization in **3a** is consistent with the extremely acute Co−C2−N1 and Co−N1−C2 angles of 69° and 66°, respectively. Furthermore, N3 (*trans* to Co−N1) and the axial chloride also participate in significant delocalization interactions, as shown in Figure 6.

https://doi.org/10.1021/acs.organomet.4c00113
Organometallics 2024, 43, 1057−1067

Donor NBO [Hybridization; Occupancy]	Acceptor NBO [Hybridization; Occupancy]	E(2) (kcal/mol)
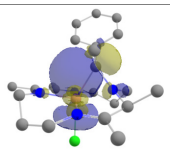 σ_{Co-C} [42% Co($sd^{2.01}$) + 58% C($sp^{5.89}$); 1.71]	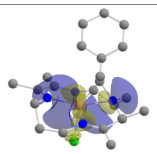 σ^*_{Co-N1} [80% Co($sd^{2.08}$) + 20% N($sp^{7.78}$); 0.50]	106
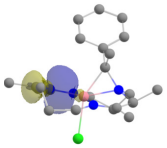 LP_{N3} [$sp^{2.23}$; 1.66]	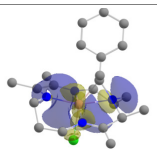 σ^*_{Co-N1} [80% Co($sd^{2.08}$) + 20% N($sp^{7.78}$); 0.50]	70
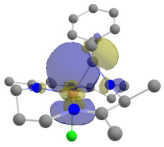 σ_{Co-C} [42% Co($sd^{2.01}$) + 58% C($sp^{5.89}$); 1.71]	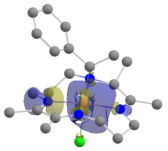 σ^*_{Co-N4} [82% Co($sd^{1.98}$) + 18% N($sp^{2.46}$); 0.40]	67
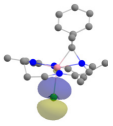 LP_{Cl} [$sp^{5.4}$; 1.73]	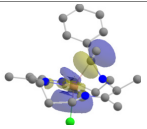 σ^*_{Co-C} [58% Co($sd^{2.01}$) + 42% C($sp^{5.89}$); 0.37]	66
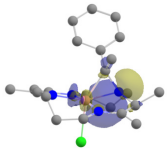 σ_{Co-N1} [20% Co($sd^{2.08}$) + 80% N($sp^{7.78}$); 1.84]	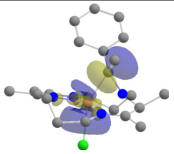 σ^*_{Co-C} [58% Co($sd^{2.01}$) + 42% C($sp^{5.89}$); 0.37]	53

Figure 6. Most significant donor → acceptor NBO interactions in **3a** are relevant to the (C2−Co−N1) metallacycle. Orbitals are plotted at | isovalue| = 0.035 au.

■ CONCLUSIONS

The reaction between $[Co^{III}(TIM)Cl_2]^+$ and terminal aryl alkynes in the presence of $NaBH_4$ generated the first examples of Co^{III}(TIM) based mono- (**1**) and bis- (**2**) alkenyl complexes. Moreover, the addition of a hydride to the TIM macrocycle enables the formation of a 1-aza-2cobalt-cyclo-propane-bearing species (**3**). Among the three unique classes of products, significant differences in the structural and electronic properties were revealed via X-ray diffraction studies, UV−vis and ^{1}H NMR spectroscopies, and cyclic voltammetry. The photophysical properties, reactivity and catalytic activities of these novel organocobalt(III) complexes will be evaluated in future studies inspired by organic transformations mediated by vitamin B_{12} and its model complexes.[45]

■ EXPERIMENTAL SECTION

Materials. Phenylacetylene and sodium borohydride were purchased from Oakwood Chemical. Dry acetonitrile used in the electrochemical studies was purchased from Thermo Scientific. All of the reagents were used as received. The starting complex, $[Co(TIM)Cl_2]PF_6$, was prepared according to literature reports.[43] Also synthesized according to literature were 1-ethynyl-4-*tert*-butylbenzene ($HC_2C_6H_4$-4-^{t}Bu)[46,47] and 1-ethynyl-2,3,4,5,6-pentafluorobenzene ($HC_2C_6F_5$).[48]

Physical Measurements. Electronic absorption spectra were recorded on a JASCO V-780 UV−vis−NIR spectrophotometer. ^{1}H NMR spectra were collected by using a Varian INOVA300 MHz spectrometer or Bruker NEO300 MHz. Cyclic voltammograms were collected on a CHI620A voltammetric analyzer, with a Pt-wire auxiliary electrode, glassy carbon working electrode (diameter = 2 mm; area = 3.14 mm^2), and a Ag/AgCl pseudoreference electrode. The working electrode was polished with alumina (0.05 μm) as needed. Voltammograms were collected on 1.0 mM solutions of the appropriate complex in dry acetonitrile at a 0.1 M electrolyte (*n*-Bu_4PF_6) concentration. An Advion Mass Spectrometer was used for the ESI-MS analysis. Elemental analyses were performed by Atlantic Microlabs, Inc. in Norcross, GA. All air-sensitive reactions were performed using standard Schlenk line techniques using a dry N_2 atmosphere.

Computational Details. DFT calculations were performed using Gaussian16 rev C.01.[49] Orbitals were plotted and visualized using either Gaussview 6[50] or Chemcraft.[51] Input geometries for **1a−3a** were obtained from their respective crystal structures. The functionals B3LYP,[52−55] BP86,[56,57] PBE0,[58,59] CAM-B3LYP,[60] and M06-L[61] were tested for geometry optimization and frequency analyses. The best agreement with experimental bond metrics were obtained with the B3LYP functional along with Grimme's GD3-BJ[62] dispersion

https://doi.org/10.1021/acs.organomet.4c00113
Organometallics 2024, 43, 1057−1067

correction. The def2tzvp basis set[63,64] was used for Co, C, N, and Cl atoms, and the 6-31G* basis set for H atoms. All calculations were done applying a polarizable continuum solvent model (CPCM;[65,66] acetonitrile) to compare to experimental spectra obtained in the same solvent. Single point energy calculations were then repeated using the M06-L functional, which gave better agreement with the optical and electrochemical HOMO−LUMO gaps. In all cases, time dependent DFT (TDDFT) calculations were performed to validate our computational methodology. UV−vis spectra calculated using the M06-L functional were found to be in excellent agreement with experiment (see Figures S17−S19). This functional was thus used in all further calculations.

Natural bond orbital calculations were carried out using the NBO7 package[67] as implemented in Gaussian16 rev. C.01. The default Lewis structures generated by NBO were found to be unsatisfactory, so all NBO calculations were "guided" using chemically reasonable Lewis structures provided using the $CHOOSE keylist. The keylists and atom numbering schemes are provided in the Supporting Information. Individual atom contributions to canonical MOs were calculated in the natural atomic orbital (NAO) basis using the NAOMO keyword, and the output was analyzed using Multiwfn v.3.8.[68]

Syntheses. *Synthesis of [Co(TIM)(C(CH$_2$)Ph)Cl]PF$_6$ (**1a**), [Co(TIM(C(CH$_2$)Ph)$_2$]PF$_6$ (**2a**), and [Co(TIM″)(C(CH$_3$)Ph)Cl]PF$_6$ (**3a**).* [Co(TIM)Cl$_2$]PF$_6$ (421.1 mg g, 0.803 mmol) was dissolved in 100 mL of a 4/1 acetone/CH$_3$OH solution. The blue-green solution was purged with N_2 prior to the addition of HC$_2$Ph (0.45 mL, 4.1 mmol). Upon the addition of $NaBH_4$ (69.0 mg, 1.82 mmol), the reaction mixture immediately turned purple and then blue before a green color persisted. After 5 h, the reaction was opened to air resulting in a color change to red-brown. This was filtered through a fritted funnel to remove precipitated Na^+ salts. The filtrate was collected and the solvent was removed. The remaining sludge was taken up in CH_2Cl_2 and loaded onto a silica gel column. A 1/49 CH$_3$OH/CH_2Cl_2 solvent mixture was used to elute the three fractions. The fractions were collected, and the solvent was removed. Independent recrystallization of each fraction using CH_3CN and diethyl ether afforded the products as a light yellow-orange (fraction 1; **2a**), orange (fraction 2; **1a**), or red-orange (fraction 3; **3a**) powder.

*Yield of **1a**.* 67.0 mg (0.113 mmol; 14%). ESI-MS (positive ions, formula $C_{22}H_{31}ClCoN_4PF_6$, MW 590.87): m/z (%) = 445.2 (100, calcd for [**1a**]$^+$ 445.9). Visible spectrum, λ_{max} (nm, ε (M^{-1} cm^{-1})): 477 (1310), 371 (2550). ^{1}H NMR (300 MHz, CD_3CN) δ 7.24−7.13 (m, 3H), 6.66−6.61 (m, 2H), 4.25 (d, 1H, J = 1.7 Hz), 3.86 (dd, 5H, J = 17.6, 4.7 Hz), 3.72−3.61 (m, 4H), 2.39 (dtd, 2H, J = 8.6, 6.0, 3.2 Hz), 2.30−2.21 (m, 14H). Elem. Anal. Found (calcd) for $CoC_{22.5}H_{33}N_4PF_6Cl_2O_{0.5}$ (**1a**·0.5CH_2Cl_2·0.5H_2O): C 42.17 (42.07); H 5.22 (5.18); N 9.03 (8.72).

*Yield of **2a**.* 20.3 mg (0.031 mmol, 4%). ESI-MS (positive ions, formula $C_{30}H_{38}CoF_6N_4P$, MW 658.56): m/z (%) = 513.2 (100, calcd for [**2a**]$^+$ 513.2). Visible spectrum, λ_{max} (nm, ε (M^{-1} cm^{-1})): 406 (5430), 300 (18,700). ^{1}H NMR (300 MHz, CD_3CN) δ 7.10 (m, 6H), 6.45−6.36 (m, 4H), 4.97 (s, 2H), 3.81 (s, 2H), 3.54−3.47 (m, 8H), 2.08 (t, 4H, J = 3.5 Hz), 1.98 (t, 12H, J = 1.0 Hz). Elem. Anal. Found (calcd) for $CoC_{30.5}H_{40}N_4PF_6ClO_{0.5}$ (**2a**·0.5CH_2Cl_2·0.5H_2O): C 51.58 (51.59); H 5.60 (5.68); N 8.07 (7.89).

*Yield of **3a**.* 47.0 mg (0.079 mmol, 10%). ESI-MS (positive ions, formula $C_{22}H_{33}ClCoF_6N_4P$, MW 592.88): m/z (%) = 447.2 (100, calcd for [**3a**]$^+$ 447.2). Visible spectrum, λ_{max} (nm, ε (M^{-1} cm^{-1})): 512 (1470). ^{1}H NMR (300 MHz, CD_3CN) δ 7.21 (d, 5H, J = 27.6 Hz), 4.65 (s, 1H), 4.23 (d, 1H, J = 15.7 Hz), 4.04 (t, 1H, J = 13.8 Hz), 3.92−3.79 (m, 2H), 3.49−3.36 (m, 3H), 3.18−2.98 (m, 3H), 2.49 (t, 3H, J = 1.4 Hz), 2.27 (s, 2H), 2.04 (s, 6H), 1.73 (d, 3H, J = 7.3 Hz), 1.07 (s, 3H). Elem. Anal. Found (calcd) for $CoC_{22}H_{34}N_4PF_6ClO_{0.5}$ (**3a**·0.5H_2O): C 43.99 (43.90); H, 5.57 (5.69); N, 9.44 (9.31).

*Synthesis of [Co(TIM)(C(CH$_2$)C$_6$H$_4$-4-^{t}Bu)Cl]PF$_6$ (**1b**) and [Co(TIM″)(C(CH$_3$)C$_6$H$_4$-4-^{t}Bu)Cl]PF$_6$ (**3b**).* [Co(TIM)Cl$_2$]PF$_6$ (350.1 mg, 0.673 mmol) and HC$_2$C$_6$H$_4$-4-^{t}Bu (1.98 mmol) were combined in 100 mL of a 4/1 acetone/CH$_3$OH solution. The blue-green solution was purged with N_2 prior to the addition of $NaBH_4$ (51.2 mg, 1.35 mmol). The reaction mixture turned dark brown within 1 min before turning dark red. The reaction was stirred for 6 h before opening to air and filtering through a fritted funnel to remove the excess Na^+ salts. The red filtrate was collected, and the solvent was removed *in vacuo*. The sludge was taken up in CH_3CN, and the addition of diethyl ether produced a brown solid. The solid was collected and washed with diethyl ether. Purification over a silica column plug using a 24/1 CH_2Cl_2/CH$_3$OH mixture eluted a brown-orange fraction. Increasing the polarity to 9/1 CH_2Cl_2/CH$_3$OH eluted a red band. The fractions were collected and concentrated. The addition of diethyl ether afforded **1b** as a pale orange solid (fraction 1) and **3b** as a red microcrystalline solid (fraction 2).

*Yield of **1b**.* 25.2 mg (0.039 mmol, 5.7%). ESI-MS (positive ions, formula $C_{26}H_{39}ClCoF_6N_4P$, MW 646.97): m/z (%) = 501.2 (100, calcd for [**1b**]$^+$ 501.2). Visible spectrum, λ_{max} (nm, ε (M^{-1} cm^{-1})): 478 (1010), 380 (2700), 270 (16,000). ^{1}H NMR (300 MHz, CD_3CN) δ 7.24−7.16 (m, 2H), 6.56 (d, 2H, J = 8.1 Hz), 4.24 (d, 1H, J = 1.6 Hz), 4.06 (s, 5H), 3.84 (dd, 4H, J = 15.0, 4.3 Hz), 3.67 (s, 2H), 2.70 (s, 3H), 2.51 (s, 3H), 2.26 (s, 6H), 2.06 (s, 1H), 1.61 (s, 1H), 1.28 (s, 9H). Elem. Anal. Found (calcd) for $CoC_{30}H_{49}N_5PF_6Cl_3O_{2.5}$ (**1b**·2.5H_2O·CH$_3$CN·CH_2Cl_2): C 43.45 (43.41); H, 5.90 (5.95); N, 8.76 (8.44).

*Yield of **3b**.* 113.0 mg (0.174 mmol, 26%). ESI-MS (positive ions, formula $C_{26}H_{41}ClCoF_6N_4P$, MW 648.99): m/z (%) = 503.2 (100, calcd for [**3b**]$^+$ 503.2). Visible spectrum, λ_{max} (nm, ε (M^{-1} cm^{-1})): 513 (1720). ^{1}H NMR (300 MHz, CD_3CN) δ 7.38−7.17 (m, 3H), 6.56 (d, 1H, J = 8.3 Hz), 4.64 (s, 1H), 4.22 (d, 1H, J = 14.8 Hz), 4.11−3.98 (m, 1H), 3.90−3.78 (m, 2H), 3.50−3.30 (m, 4H), 3.10 (t, 2H, J = 14.1 Hz), 2.49 (d, 3H, J = 1.5 Hz), 2.26 (s, 2H), 2.02 (d, 6H, J = 6.3 Hz), 1.73 (dd, 3H, J = 7.3, 2.1 Hz), 1.28 (d, 9H, J = 2.9 Hz), 1.06 (s, 3H). Elem. Anal. Found (calcd) for $CoC_{26}H_{43}N_4PF_6ClO$ (**3b**·H_2O): C 46.67 (46.82); H, 6.24 (6.50); N, 8.55 (8.40).

*Synthesis of [Co(TIM)(C(CH$_2$)C$_6$F$_5$)Cl]PF$_6$ (**1c**) and [Co(TIM)(C(CH$_2$)C$_6$F$_5$)$_2$]PF$_6$ (**2c**).* In a 100 mL flask, [Co(TIM)Cl$_2$]PF$_6$ (173.7 mg, 0.333 mmol) and HC$_2$C$_6$F$_5$ (1.00 mmol) were combined in 50 mL of a 4/1 acetone/CH$_3$OH solution. The blue-green solution was purged with N_2 for 15 min prior to the addition of $NaBH_4$ (25.0 mg, 0.667 mmol). The reaction mixture immediately turned purple before rapidly turning blue within a minute. The reaction mixture began turning dark green over the next hour and was stirred for 2 h before opening to air. The solution became a red-orange color and was filtered through a fritted funnel to remove the excess Na^+ salts. The filtrate was collected, and the solvent was removed *in vacuo*. The sludge was taken up in CH_3CN, and the addition of diethyl ether produced a brown solid. The solid was collected and washed with diethyl ether.

Separation of **2c** was achieved by using a silica gel column. The crude product was loaded using minimal CH_2Cl_2 and eluted with a 9/1 CH_2Cl_2/acetone mixture as a light-yellow fraction. Once this band was collected, the mobile phase was changed to CH$_3$OH to elute a yellow-orange fraction. Concentration of the first yellow fraction followed by the addition of diethyl ether afforded **2c** as a pale yellow solid. Yield of **2c**: 12.4 mg (0.015 mmol, 4.5%). ESI-MS (positive ions, formula $C_{30}H_{28}CoF_{16}N_4P$, MW 838.46): m/z (%) = 693.2 (100, calcd for [**2c**]$^+$ = 693.1). Visible spectrum, λ_{max} (nm, ε (M^{-1} cm^{-1})): 275 (24,000). ^{1}H NMR (300 MHz, CD_3CN) δ 5.21 (s, 2H), 4.34 (s, 2H), 3.56 (t, J = 5.4 Hz, 8H), 2.52−2.41 (m, 4H), 2.29 (s, 12H). Elem. Anal. Found (calcd) for $CoC_{38}H_{39}N_5PF_{16}Cl_6O$ (**2c**·H_2O·CH$_3$CN·3CH_2Cl_2): C 38.41 (38.41); H 3.24 (3.31); N 6.17 (5.89).

Concentration of the yellow-orange fraction followed by the addition of diethyl ether afforded **1c** and *trans*-[Co(TIM″)(C(CH$_2$)C$_6$F$_5$)Cl]PF$_6$ (**1c′**) in a mixture. Further purification over silica was unsuccessful at separating **1c** from **1c′** due to their near identical R_f values across numerous mobile phases.

X-ray Crystallographic Analysis. Single crystals were grown from the slow diffusion of diethyl ether into concentrated solutions of the appropriate compound in CH_3CN (**1a**, **1c′**, and **3a**), CH_2Cl_2 (**1c**), or 1:1 acetone/CH_2Cl_2 (**2c**). Single crystals of **2a** were grown from the slow evaporation of a concentrated CH_3CN solution. X-ray diffraction data were obtained on a Bruker Quest diffractometer with

https://doi.org/10.1021/acs.organomet.4c00113
Organometallics 2024, 43, 1057−1067

Mo Kα radiation (λ = 0.71073 Å) at 150 K for **1a**, **1c**′, and **3a** and with Cu Kα radiation (λ = 1.54178 Å) at 150 K for **1c**, **2a**, and **2c**. Data were collected; reflections were indexed and processed using APEX4[69] and reduced using SAINT. The space groups were assigned, and the structures were solved by direct methods using XPREP within the SHELXTL suite of programs,[70] solved using ShelXT,[71] and refined using Shelxl[72,73] and Shelxle.[74]

■ ASSOCIATED CONTENT

Supporting Information

The Supporting Information is available free of charge at https://pubs.acs.org/doi/10.1021/acs.organomet.4c00113.

Additional synthetic details, details of X-ray diffraction studies, absorption spectra for **1b**, **2a**, and **3b**, ^{1}H NMR spectra, cyclic voltammograms of **1b**, **2a**, and **3b**, and computational details (PDF)

Cartesian coordinates for [**1a**]$^+$, [**2a**]$^+$, and [**3a**]$^+$ (XYZ)

Accession Codes

CCDC 2325683−2325687 and 2326269 contain the supplementary crystallographic data for this paper. These data can be obtained free of charge via www.ccdc.cam.ac.uk/data_request/cif, or by emailing data_request@ccdc.cam.ac.uk, or by contacting The Cambridge Crystallographic Data Centre, 12 Union Road, Cambridge CB2 1EZ, UK; fax: +44 1223 336033.

■ AUTHOR INFORMATION

Corresponding Author

Tong Ren − *Department of Chemistry, Purdue University, West Lafayette, Indiana 47906, United States;* orcid.org/0000-0002-1148-0746; Email: tren@purdue.edu

Authors

Leobardo Rodriguez Segura − *Department of Chemistry, Purdue University, West Lafayette, Indiana 47906, United States*

Kyle J. McGuire − *Department of Chemistry, Purdue University, West Lafayette, Indiana 47906, United States*

Adharsh Raghavan − *Department of Chemistry, Purdue University, West Lafayette, Indiana 47906, United States;* orcid.org/0000-0002-4550-6262

Jeremy J. Roos − *Department of Chemistry, Purdue University, West Lafayette, Indiana 47906, United States*

Complete contact information is available at: https://pubs.acs.org/10.1021/acs.organomet.4c00113

Notes

The authors declare no competing financial interest.

■ ACKNOWLEDGMENTS

This material is based upon work supported by the U.S. National Science Foundation (CHE 2102049).

■ REFERENCES

(1) Wheelhouse, K. M. P.; Webster, R. L.; Beutner, G. L. Advances and Applications in Catalysis with Earth-Abundant Metals. *Org. Process Res. Dev.* **2023**, *27*, 1157−1159.

(2) Hayler, J. D.; Leahy, D. K.; Simmons, E. M. A Pharmaceutical Industry Perspective on Sustainable Metal Catalysis. *Organometallics* **2019**, *38*, 36−46.

(3) Chirik, P. J.; Wieghardt, K. Radical Ligands Confer Nobility on Base-Metal Catalysts. *Science* **2010**, *327*, 794−795.

(4) Arevalo, R.; Chirik, P. J. Enabling Two-Electron Pathways with Iron and Cobalt: From Ligand Design to Catalytic Applications. *J. Am. Chem. Soc.* **2019**, *141*, 9106−9123.

(5) Chirik, P. J. Iron- and Cobalt-Catalyzed Alkene Hydrogenation: Catalysis with Both Redox-Active and Strong Field Ligands. *Acc. Chem. Res.* **2015**, *48*, 1687−1695.

(6) Fitzsimmons, M. C.; Yessengazin, A.; Hatzis, G. P.; Stevens, J. E.; Moore, C. E.; Thomas, C. M. Catalytic Hydrogenation of Terminal Alkenes by a (PPP) Pincer-Ligated Cobalt(II) Complex. *Organometallics* **2023**, *42*, 1439−1443.

(7) Guo, J.; Cheng, Z.; Chen, J.; Chen, X.; Lu, Z. Iron- and Cobalt-Catalyzed Asymmetric Hydrofunctionalization of Alkenes and Alkynes. *Acc. Chem. Res.* **2021**, *54*, 2701−2716.

(8) Epping, R. F. J.; Vesseur, D.; Zhou, M.; de Bruin, B. Carbene Radicals in Transition-Metal-Catalyzed Reactions. *ACS Catal.* **2023**, *13*, 5428−5448.

(9) Tok, G. C.; Reiter, S.; Freiberg, A. T. S.; Reinschlüssel, L.; Gasteiger, H. A.; de Vivie-Riedle, R.; Hess, C. R. H2 Evolution from Electrocatalysts with Redox-Active Ligands: Mechanistic Insights from Theory and Experiment vis-à-vis Co-Mabiq. *Inorg. Chem.* **2021**, *60*, 13888−13902.

(10) Esezobor, O. Z.; Zeng, W.; Niederegger, L.; Grubel, M.; Hess, C. R. Co−Mabiq Flies Solo: Light-Driven Markovnikov-Selective C- and N-Alkylation of Indoles and Indazoles without a Cocatalyst. *J. Am. Chem. Soc.* **2022**, *144*, 2994−3004.

(11) Malme, J. T.; Clendening, R. A.; Ash, R.; Curry, T.; Ren, T.; Vura-Weis, J. Nanosecond Metal-to-Ligand Charge-Transfer State in an Fe(II) Chromophore: Lifetime Enhancement via Nested Potentials. *J. Am. Chem. Soc.* **2023**, *145*, 6029−6034.

(12) Glaser, F.; Aydogan, A.; Elias, B.; Troian-Gautier, L. The great strides of iron photosensitizers for contemporary organic photoredox catalysis: On our way to the holy grail? *Coord. Chem. Rev.* **2024**, *500*, No. 215522.

(13) Hess, C. R.; Weyhermuller, T.; Bill, E.; Wieghardt, K. [{Fe(tim)}2]: An Fe-Fe Dimer Containing an Unsupported Metal-Metal Bond and Redox-Active N4Macrocyclic Ligands. *Angew. Chem., Int. Ed.* **2009**, *48*, 3703−3706.

(14) Hess, C. R.; Weyhermuller, T.; Bill, E.; Wieghardt, K. Influence of the Redox Active Ligand on the Reactivity and Electronic Structure of a Series of Fe(TIM) Complexes. *Inorg. Chem.* **2010**, *49*, 5686−5700.

(15) Rodriguez Segura, L.; Lee, S. A.; Mash, B. L.; Schuman, A. J.; Ren, T. A Series of Mono- and Bis-Alkynyl Co(III) Complexes Supported by a Tetra-imine Macrocyclic Ligand (TIM). *Organometallics* **2021**, *40*, 3313−3322.

(16) Rodriguez Segura, L.; Cox, K. E.; Samayoa-Oviedo, H. Y.; Ren, T. Further Studies of CoIII(TIM) Mono-Alkynyl and Bis-Alkynyl Complexes. *Eur. J. Inorg. Chem.* **2023**, *2023*, No. e202200641.

(17) Rodriguez Segura, L.; Ren, T. Formation of an Aza-Cobalt-Cyclobutene on CoIII(TIM): Hidden Noninnocence of the TIM Ligand. *Organometallics* **2022**, *41*, 1130−1133.

(18) Rodriguez Segura, L.; Clendening, R. A.; Ren, T. Further Exploration of Aza-Cobalt-Cyclobutenes on CoIII(TIM) Complexes: Reactivity and Spectroelectrochemistry. *Organometallics* **2023**, *42*, 1717−1724.

(19) Richards, C. A.; Rath, N. P.; Neely, J. M. Carbene-Like Reactivity in an Iron Azametallacyclobutene Complex: Insights from Electronic Structure. *Inorg. Chem.* **2022**, *61*, 13266−13270.

(20) Richards, C. A.; Rath, N. P.; Neely, J. M. Isolation and Reactivity of an Iron Azametallacyclobutene Complex. *Organometallics* **2022**, *41*, 1763−1768.

(21) Demarteau, J.; Debuigne, A.; Detrembleur, C. Organocobalt Complexes as Sources of Carbon-Centered Radicals for Organic and Polymer Chemistries. *Chem. Rev.* **2019**, *119*, 6906−6955.

(22) Jana, S.; Mayerhofer, V. J.; Teskey, C. J. Photo- and Electrochemical Cobalt Catalysed Hydrogen Atom Transfer for the Hydrofunctionalisation of Alkenes. *Angew. Chem., Int. Ed.* **2023**, *62*, No. e202304882.

(23) Perry, C. B.; Shin, N.; Fernandes, M. A.; Marques, H. M. Phenylvinylcobalamin: an alkenylcobalamin featuring a ligand with a large trans influence. *Dalton Trans.* **2013**, *42*, 7555−7561.
(24) Wang, Z.; Yao, Z.; Lyu, Z.; Xiong, Q.; Wang, B.; Fu, X. Thermodynamic and reactivity studies of a tin corrole-cobalt porphyrin heterobimetallic complex. *Chem. Sci.* **2018**, *9*, 4999−5007.
(25) Schrauzer, G. N.; Windgassen, R. J. Cobalamin Model Compounds. Preparation and Reactions of Substituted Alkyl- and Alkenylcobaloximes and Biochemical Implications. *J. Am. Chem. Soc.* **1967**, *89*, 1999−2007.
(26) Naumberg, M.; N-V-Duong, K.; Gaudemer, A. Mise en evidence de l'hydrure des cobaloximes(I). *J. Organomet. Chem.* **1970**, *25*, 231−242.
(27) Farmery, K.; Busch, D. H. An alkylcobalt(I) intermediate in the formation of trans-dialkylcobalt(III) complexes of two tetradentate macrocyclic ligands. *J. Chem. Soc., Chem.Commun.* **1970**, 1091−1091.
(28) Costa, G.; Mestroni, G.; Licari, T.; Mestroni, E. New sigma-bonded bisalkyl and alkyl-aryl cobalt complexes of bis-(diacetylmonoxime-imino)propane 1.3. *Inorg. Nucl. Chem. Lett.* **1969**, *5*, 561−563.
(29) Polson, S. M.; Hansen, L.; Marzilli, L. G. Novel Chemistry of Carbon Bound to Cobalt in Organocobalt Complexes Related to B12. *J. Am. Chem. Soc.* **1996**, *118*, 4804−4808.
(30) Marzilli, L. G.; Polson, S. M.; Hansen, L.; Moore, S. J.; Marzilli, P. A. B12 Models with Highly Distorted N4 Equatorial Ligation and a Co-C-N Ring: Structural Assessment of the Steric Influence of Benzimidazole and Imidazole Axial Ligands. *Inorg. Chem.* **1997**, *36*, 3854−3860.
(31) Dreos, R.; Felluga, A.; Nardin, G.; Randaccio, L.; Tauzher, G. Organometallic Complexes Containing a Co-N-C Three-Membered Ring: Factors Affecting the Dynamic of the Ring Closure. *Organometallics* **2003**, *22*, 2486−2491.
(32) Dreos, R.; Felluga, A.; Nardin, G.; Randaccio, L.; Siega, P.; Tauzher, G. A New Organocobalt Complex Containing a Co-N-C Three Membered Ring. *Inorg. Chem.* **2001**, *40*, 5541−5546.
(33) Hartshorn, R. M.; Telfer, S. G. The photodecarboxylation of [N,N-bis(2-pyridylmethyl)amino acidato]phenanthrolinecobalt(III) complexes: -formation and decomposition of metallacyclic species. *J. Chem. Soc., Dalton Trans.* **2000**, 2801−2808.
(34) Otter, C. A.; Hartshorn, R. M. Preparation and photochemistry of cobalt(iii) amino and amino acidato complexes containing tripodal polypyridine ligands. *Dalton Trans.* **2004**, 150−156.
(35) Poznyak, A. L.; Pavlovski, V. I.; Chuklanova, E. B.; Polynova, T. N.; Porai-Koshits, M. A. New type of organocobalt complexes structure of n2-aminomethylenebis(2,2'-bipyridyl) cobalt (III). *Monatsh. Chem.* **1982**, *113*, 561−564.
(36) Tonei, D. M.; Baker, L.-J.; Brothers, P. J.; Clark, G. R.; Ware, D. C. Decarboxylation of an α-amino acid coordinated to cobalt(III): kinetic stabilisation and molecular structure of a Co−C−N three-membered ring incorporated into a cobalt(III) macrocyclic ligand complex. *Chem. Commun.* **1998**, 2593−2594.
(37) Brookhart, M.; Studabaker, W. B. Cyclopropanes from reactions of transition metal carbene complexes with olefins. *Chem. Rev.* **1987**, *87*, 411−432.
(38) Mahy, J. P.; Battioni, P.; Bedi, G.; Mansuy, D.; Fischer, J.; Weiss, R.; Morgenstern-Badarau, I. Iron-porphyrin-nitrene complexes: preparation, properties, and crystal structure of porphyrin-iron(III) complexes with a tosylnitrene inserted into an iron-nitrogen bond. *Inorg. Chem.* **1988**, *27*, 353−359.
(39) Liu, J.; Hu, L.; Wang, L.; Chen, H.; Deng, L. An Iron(II) Ylide Complex as a Masked Open-Shell Iron Alkylidene Species in Its Alkylidene-Transfer Reactions with Alkenes. *J. Am. Chem. Soc.* **2017**, *139*, 3876−3888.
(40) Michaely, W. J.; Schrauzer, G. N. Reactions of vinyl ethers with cobalamins and cobaloximes. *J. Am. Chem. Soc.* **1973**, *95*, 5771−5772.
(41) Smalley, T. L. J.; Wright, M. W.; Garmon, S. A.; Welker, M. E.; Rheingold, A. L. Synthesis of 2-transition-metal-substituted 1,3-butadienyl complexes with unusual structures and facile Diels-Alder reactions of cobalt 1,3-butadiene complexes. *Organometallics* **1993**, *12*, 998−1000.
(42) Randaccio, L.; Geremia, S.; Nardin, G.; Wuerges, J. X-ray structural chemistry of cobalamins. *Coord. Chem. Rev.* **2006**, *250*, 1331−1350.
(43) Jackels, S. C.; Farmery, K.; Barefield, E. K.; Rose, N. J.; Busch, D. H. Tetragonal cobalt(III) complexes containing tetradentate macrocyclic amine ligands with different degrees of unsaturation. *Inorg. Chem.* **1972**, *11*, 2893−2901.
(44) Mayer, I. Charge, bond order and valence in the AB initio SCF theory. *Chem. Phys. Lett.* **1983**, *97*, 270−274.
(45) Wdowki, T.; Gryko, D. C−C Bond Forming Reactions Enabled by Vitamin B12—Opportunities and Challenges. *ACS Catal.* **2022**, *12*, 6517−6531.
(46) Brizius, G.; Bunz, U. H. F. Increased Activity of in Situ Catalysts for Alkyne Metathesis. *Org. Lett.* **2002**, *4*, 2829−2831.
(47) Diao, Y.; Hu, J.; Cheng, S.; Ma, F.; Li, M.-Q.; Hu, X.; Li, Y. Y.; He, J.; Xu, Z. Dense Alkyne Arrays of a Zr(IV) Metal-Organic Framework Absorb Co2(CO)8 for Functionalization. *Inorg. Chem.* **2020**, *59*, 5626−5631.
(48) Zhang, Y.; Wen, J. A Convenient Synthesis of Bis-(polyfluorophenyl)butadiyne Monomers. *Synthesis* **1990**, *1990*, 727−728.
(49) *Gaussian 16*, Revision C.01; Frisch, M. J.; Trucks, G. W.; Schlegel, H. B.; Scuseria, G. E.; Robb, M. A.; Cheeseman, J. R.; Scalmani, G.; Barone, V.; Petersson, G. A.; Nakatsuji, H.; Li, X.; Caricato, M.; Marenich, A. V.; Bloino, J.; Janesko, B. G.; Gomperts, R.; Mennucci, B.; Hratchian, H. P.; Ortiz, J. V.; Izmaylov, A. F.; Sonnenberg, J. L.; Williams-Young, D.; Ding, F.; Liarrarini, F.; Egidi, F.; Goings, J.; Peng, B.; Petrone, A.; Henderson, T.; Ranasinghe, D.; Zakrzewski, V. G.; Gao, J.; Rega, N.; Zheng, G.; Liang, W.; Hada, M.; Ehara, M.; Toyota, K.; Fukuda, R.; Hasegawa, J.; Ishida, M.; Nakajima, T.; Honda, Y.; Kitao, O.; Nakai, H.; Vreven, T.; Throssell, K.; Montgomery, J. A., Jr.; Peralta, J. E.; Ogliaro, F.; Bearpark, M. J.; Heyd, J. J.; Brothers, E. N.; Kudin, K. N.; Staroverov, V. N.; Keith, T. A.; Kobayashi, R.; Normand, J.; Raghavachari, K.; Rendell, A. P.; Burant, J. C.; Iyengar, S. S.; Tomasi, J.; Cossi, M.; Millam, J. M.; Klene, M.; Adamo, C.; Cammi, R.; Ochterski, J. W.; Martin, R. L.; Morokuma, K.; Farkas, O.; Foresman, J. B.; Fox, D. J.; Gaussian, Inc.: Wallingford, CT, 2016.
(50) *GaussView*, Version 6.1; Dennington, R.; Keith, T. A.; Millam, J. M.; Semichem Inc.: Shawnee Mission, KS, 2016.
(51) *Chemcraft - graphical program for visualization of quantum chemistry computations*. Version 1.8, build 654; Zhurko, G. A.: Ivanovo, Russia, 2005.
(52) Becke, A. D. Density-functional thermochemistry. III. The role of exact exchange. *J. Chem. Phys.* **1993**, *98*, 5648−5652.
(53) Lee, C.; Yang, W.; Parr, R. G. Development of the Colle-Salvetti correlation-energy formula into a functional of the electron density. *Phys. Rev. B* **1988**, *37*, 785−789.
(54) Vosko, S. H.; Wilk, L.; Nusair, M. Accurate spin-dependent electron liquid correlation energies for local spin density calculations: a critical analysis. *Can. J. Phys.* **1980**, *58*, 1200−1211.
(55) Stephens, P. J.; Devlin, F. J.; Chabalowski, C. F.; Frisch, M. J. Ab initio calculation of vibrational absorption and circular dichroism spectra using density functional force fields. *J. Phys. Chem.* **1994**, *98*, 11623−11627.
(56) Perdew, J. P. Density-functional approximation for the correlation energy of the inhomogeneous electron gas. *Phys. Rev. B* **1986**, *33*, 8822−8824.
(57) Becke, A. D. Density-functional exchange-energy approximation with correct asymptotic behavior. *Phys. Rev. A* **1988**, *38*, 3098−3100.
(58) Perdew, J. P.; Burke, K.; Ernzerhof, M. Generalized Gradient Approximation Made Simple. *Phys. Rev. Lett.* **1996**, *77*, 3865−3868.
(59) Perdew, J. P.; Burke, K.; Ernzerhof, M. Generalized Gradient Approximation Made Simple [Phys. Rev. Lett. 77, 3865 (1996)]. *Phys. Rev. Lett.* **1997**, *78*, 1396.

https://doi.org/10.1021/acs.organomet.4c00113
Organometallics 2024, 43, 1057−1067

(60) Yanai, T.; Tew, D. P.; Handy, N. C. A new hybrid exchange−correlation functional using the Coulomb-attenuating method (CAM-B3LYP). *Chem. Phys. Lett.* **2004**, *393*, 51−57.
(61) Zhao, Y.; Truhlar, D. G. A new local density functional for main-group thermochemistry, transition metal bonding, thermochemical kinetics, and noncovalent interactions. *J. Chem. Phys.* **2006**, *125*, No. 194101.
(62) Grimme, S.; Ehrlich, S.; Goerigk, L. Effect of the damping function in dispersion corrected density functional theory. *J. Comput. Chem.* **2011**, *32*, 1456−1465.
(63) Weigend, F.; Ahlrichs, R. Balanced basis sets of split valence, triple zeta valence and quadruple zeta valence quality for H to Rn: Design and assessment of accuracy. *Phys. Chem. Chem. Phys.* **2005**, *7*, 3297−3305.
(64) Weigend, F. Accurate Coulomb-fitting basis sets for H to Rn. *Phys. Chem. Chem. Phys.* **2006**, *8*, 1057−1065.
(65) Barone, V.; Cossi, M. Quantum Calculation of Molecular Energies and Energy Gradients in Solution by a Conductor Solvent Model. *J. Phys. Chem. A* **1998**, *102*, 1995−2001.
(66) Cossi, M.; Rega, N.; Scalmani, G.; Barone, V. Energies, structures, and electronic properties of molecules in solution with the C-PCM solvation model. *J. Comput. Chem.* **2003**, *24*, 669−681.
(67) *NBO 7.0*; Glendening, E. D.; Badenhoop, J. K.; Reed, A. E.; Carpenter, J. E.; Bohmann, J. A.; Morales, C. M.; Karafiloglou, P.; Landis, C. R.; Weinhold, F.; Theoretical Chemistry Institute, University of Wisconsin: Madison, WI, 2018.
(68) Lu, T.; Chen, F. Multiwfn: A multifunctional wavefunction analyzer. *J. Comput. Chem.* **2012**, *33*, 580−592.
(69) *APEX4 v2022.10−1, Saint V8.40B*; Bruker AXS, Inc.: Madison, WI, 2022.
(70) *SHELXTL suite of programs, version 6.14*; Bruker AXS Inc.: Madison, WI, 2000−2003.
(71) Sheldrick, G. M. SHELXT − Integrated space-group and crystal-structure determination. *Acta Crystallogr.* **2015**, *71*, 3−8.
(72) *SHELXL2019*; Sheldrick, G. M.: Göttingen, Germany, 2019.
(73) Sheldrick, G. M. Crystal structure refinement with SHELXL. *Acta Crystallogr. C* **2015**, *71*, 3−8.
(74) Hübschle, C. B.; Sheldrick, G. M.; Dittrich, B. ShelXle: a Qt graphical user interface for SHELXL. *J. Appl. Crystallogr.* **2011**, *44*, 1281−1284.

https://doi.org/10.1021/acs.organomet.4c00113
Organometallics 2024, 43, 1057−1067